A Study of the Shapiro-Wilk Test for the Detection of Pulsed Sinusoidal Radio Frequency Interference

Baris Güner, Mark T. Frankford, and Joel T. Johnson

***Abstract*— The performance of the Shapiro-Wilk (S-W) test of normality for the detection of pulsed sinusoidal radio frequency interference in microwave radiometry is analyzed. The study is motivated by the fact that the S-W test has been shown in the statistical literature to be effective in detecting a wide variety of non-Gaussian signal types. Basic properties of the S-W test statistic are reviewed, and implementation of the test in digital hardware is discussed. Because properties of the test statistic are difficult to obtain analytically, Monte Carlo simulations are utilized to compute performance. Results show that the test can provide reasonable performance in detecting pulsed sinusoidal RFI, and that quantization of data has only a minimal impact on the sensitivity achieved. Detection performance is also compared with that of the kurtosis test for normality. It is shown that the S-W test produces comparable but degraded sensitivity compared to that of the kurtosis test in most cases while avoiding the "blind spot" associated with the kurtosis test for pulsed interferers having fifty percent duty cycle. Test performance is also shown to be improved if a-priori knowledge of expected RFI pulse lengths is incorporated.**

I. Introduction

RADIO frequency interference (RFI) is a major concern for microwave radiometer systems. Mitigating RFI contributions to radiometer observations requires methods for detecting and suppressing measured non-thermal signals. Traditional radiometer systems recording powers integrated over millisecond time scales are ineffective at detecting short duty cycle RFI that may be present only for a fraction of the integration period. The incorporation of digital backends into the radiometer system [1]-[5] allows detection algorithms to be implemented using high sample rate measured field data and field properties beyond integrated power alone.

Several techniques for detecting RFI with digital backends have been proposed [2],[4],[6]-[8], and the more general theory of detection [13] shows that performance is improved as more knowledge of the RFI source is incorporated into the test design. While a-priori knowledge of the RFI sources encountered by a microwave radiometer is limited, detectors for particular classes of sources, such as pulsed or narrowband RFI, can be constructed. Alternatively, more general "omnibus" detection tests can be used to test the degree to which measured fields appear to be Gaussian random variables, as expected for the thermal noise measured by a radiometer. Several such "tests for normality" of a data sample have been studied extensively in the statistical literature (e.g. [14]-[24]).

Among tests for normality, only the kurtosis test [14]-[15] has been demonstrated to date for radiometer RFI detection [4]-[5],[8]-[11]. Studies to date have focused on pulsed-sinusoidal RFI due to the potential impact of radar interference on L-band radiometers, and the results of [4]-[5],[8]-[11] show the kurtosis test to provide high sensitivity to low duty cycle pulsed-sinusoidal sources as well as some sensitivity to continuous sinusoidal RFI. However a "blind spot" for pulses having fifty percent duty cycle was also shown for which the algorithm is insensitive to RFI, and reduced detection performance occurs for a broad range of duty cycles around fifty percent. In general, the kurtosis algorithm is insensitive to RFI sources that produce kurtosis values identical to those of a Gaussian random variable. The addition of a sixth moment test [12] has been shown to have the potential to reduce this blind spot, but only at very large RFI source powers so that the sixth moment was not generally recommended for use in [12].

This paper documents an examination of an alternate test for normality called the Shapiro-Wilk test, and compares its performance with that achieved by the kurtosis test for pulsed and continuous sinusoidal RFI. The Shapiro-Wilk test was first proposed in 1965 [16], and has been shown to be capable of detecting non-normality for a wide variety of statistical distributions, including those with Gaussian kurtosis values [17]-[18]. It has been recommended as a powerful omnibus test of normality [19]. An initial study of the Shapiro-Wilk test's performance in detecting pulsed sinusoidal RFI in comparison with two similar omnibus normality tests, those of Shapiro-Francia [20] and Chen-Shapiro [21], was provided in [22]. The results of this study generally showed that performance among these three tests is similar, so that only the Shapiro-Wilk test is examined here.

The discussion to follow considers only pulsed and continuous sinusoidal RFI sources; other RFI types may produce distinct conclusions regarding performance. In Section II, a brief review of the Shapiro-Wilk test is provided. Given the interest in performing the test in digital hardware on-board a radiometer system, test implementation is a key issue that is considered. Section III describes the Monte Carlo simulation procedure used to examine test performance, and Section IV presents results from these simulations. Shapiro-Wilk test results are compared with those achieved by the kurtosis method, and the influence of a test size parameter is also explored. Final conclusions are presented in Section V.

II. The Shapiro-Wilk test

In the following it is assumed that a microwave radiometer measures N samples of a received field, written as $y_{(i)}$ for $i = 1$ to N. Such samples are assumed to be separated by

The Ohio State University, Department of Electrical and Computer Engineering and ElectroScience Laboratory, 1320 Kinnear Road, Columbus, OH 43210, USA. Email: guner.2@osu.edu

the Nyquist sample rate of the receiver so that no correlation among samples is present in the absence of RFI.

The Shapiro-Wilk test is based on a correlation of sample "order statistics" with those of a normal distribution. The use of order statistics implies that the data sample must be sorted, with the sorted sample written in vector form as $\mathbf{y}' = (y_1, ..., y_N)$ in increasing values; here the prime $'$ is used to note the transpose of a vector. The Shapiro-Wilk test statistic W is defined as:

$$W = \frac{\left(\sum_{i=1}^{N} a_i y_i\right)^2}{\sum_{i=1}^{N}(y_i - m_1)^2} \tag{1}$$

where

$$m_1 = \frac{1}{N}\sum_{i=1}^{N} y_{(i)} \tag{2}$$

is the sample mean. W can be interpreted as a ratio of two estimates of the variance of the sample, with the estimate in the numerator only holding if the sample is drawn from a normal distribution since coefficients a_i are calculated by linear regression to the expected values of standard normal order statistics. It can be shown that W is bounded by 0 and 1, and that the expected value of W converges to 1 for Gaussian input data as the sample size is increased. The expected value of W becomes smaller as the input signal becomes non-Gaussian.

A. Expressions for the a_i coefficients

The vector of coefficients $\mathbf{a}' = (a_1, ..., a_N)$ is normalized so that $\mathbf{a}\cdot\mathbf{a}' = 1$ and is also antisymmetric, so that $a_1 = -a_N$, $a_2 = -a_{N-1}$, etc. Analytical expressions for the coefficients a_i are provided in [16], but the original forms are somewhat computationally complex. Instead empirical forms for these coefficients have been determined in terms of $u = N^{-1/2}$ as [25]:

$$\begin{aligned} a_N &= -2.706056u^5 + 4.434685u^4 - 2.071190u^3 \\ &\quad -0.147981u^2 + 0.221157u + c_N \end{aligned} \tag{3}$$

$$\begin{aligned} a_{N-1} &= -3.582633u^5 + 5.682633u^4 - 1.752461u^3 \\ &\quad -0.293762u^2 + 0.042981u + c_{N-1} \end{aligned} \tag{4}$$

$$a_i = \epsilon^{-1/2}\tilde{m}_i \tag{5}$$

with the final equation holding for $i = 3$ to $N - 2$.

In equation (5), $\tilde{\mathbf{m}}' = (\tilde{m}_1, ..., \tilde{m}_N)$ is a vector of expected values for the order statistics of the standard normal distribution, approximated by [26]-[27]:

$$\tilde{m}_i = \Phi^{-1}\{(i - 3/8)/(N + 1/4)\} \tag{6}$$

where Φ^{-1} denotes the inverse of the standard normal distribution function. Also in equation (5),

$$\epsilon = \frac{\tilde{\mathbf{m}}'\cdot\tilde{\mathbf{m}} - 2\tilde{m}_N^2 - 2\tilde{m}_{N-1}^2}{1 - 2a_N^2 - 2a_{N-1}^2} \tag{7}$$

Finally, the c_i values in equations (3) and (4) are determined from vector $\mathbf{c}' = (c_1, ..., c_N)$ by

$$\mathbf{c} = \tilde{\mathbf{m}}/(\tilde{\mathbf{m}}'\cdot\tilde{\mathbf{m}})^{1/2} \tag{8}$$

B. Implementation in digital hardware

Computation of the W statistic requires evaluation of the sample moments up to second order (for the denominator), and also a weighted sum of the sorted sample (for the numerator). It is assumed that floating point operations are not desired for an on-board digital processor, so that the numerator and denominator are recorded for computation of W in post-processing. The required sorting operation for the numerator can be accomplished either through the use of existing sort algorithms for a fixed sample size [28] or through a histogramming procedure in which counters are used to record the number of occurrences of each possible sample value. Further analysis would be required to determine which method is preferable in terms of digital resource usage.

It is assumed here that a sorting operation is used, and that the value of N is limited to a maximum of 4096 by hardware constraints. If it is desired to compute W for datasets larger than 4096 samples, it is assumed that a larger sample of size IN is split into I sub-sets of size N, for which the square root of the numerator and the denominator are separately computed. The I values for the sub-sets are then averaged, the numerator term is squared, and the result divided by the averaged denominator to obtain the W estimate for the entire sample. The impact of N in this process will be examined in Section IV-B. The coefficients a_i are fixed for a given N, so that computation of the W numerator is similar to a standard filter computation once the data sort operation is completed. While these steps are somewhat more complicated in terms of hardware implementation than purely moment based tests, overall the Shapiro-Wilk test appears to be reasonably well suited for implementation in hardware.

C. Quantization effects

When the y_i data are rounded to integer values as in a fixed point digital processor, Sheppard's correction to the variance estimate is applied by subtracting $(N-1)/12$ from the value in the denominator [29]. An examination of quantization impact on the coefficients a_i was also performed. Figure 1 plots a comparison of coefficients before and after quantization using 8-bits for $N = 4096$. The anti-symmetric nature of the a_i coefficients is apparent in the Figure, along with the increasing nature of the coefficients at large offsets from the array center. The lower plot of Figure 1 focuses on the region near the center of the coefficient array, and reveals the quantization more clearly. In the Monte Carlo simulations of Shapiro-Wilk test performance to be presented in Section IV, tests showed that the a_i coefficients for $N = 4096$ could be quantized in as few as 8 bits without a significant loss in test performance, and eight bit quantizations for these coefficients are used in all the results to be shown. The impact of quantization of the y_i data is further examined in Section IV-A.

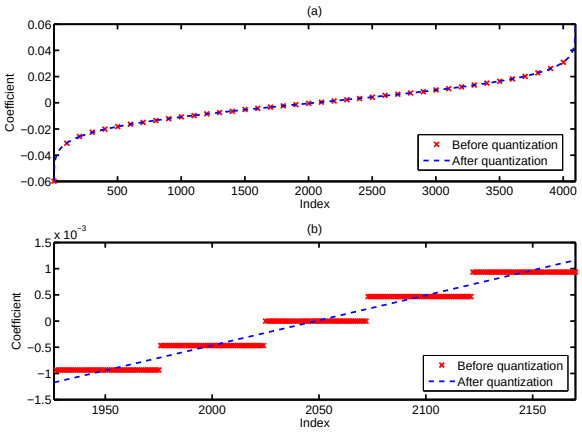

Fig. 1. Weight coefficients a_i before and after quantization using 8-bit resolution

III. Simulation Procedure

Because the W test statistic for normally distributed input data does not follow a standard probability density function (pdf), the original presentation of the Shapiro-Wilk test [16] included empirical tables of this pdf for sample sizes up to 50. Later, an approach was derived to transform W into a statistic that is approximately normal in the RFI-free case [25], [30]-[31] so that prediction of expected false-alarm rates is possible. However, tests on the simulation results described in Section IV showed this transformation to be very sensitive to quantization effects, and the transformation is not used for this reason. Instead a Monte Carlo simulation approach is applied; the probability of false alarm and probability of detection are determined by counting the number of realizations declared as RFI through a test on W in cases with no RFI present and with RFI present, respectively. Monte Carlo simulations utilized 30000 realizations in all the results to be shown, and tests with larger numbers of realizations showed negligible impact on the curves illustrated.

A. Signal model and notations

In a previous modeling study of the kurtosis test [8], received fields when pulsed sinusoidal RFI is present were modeled as uncorrelated Gaussian random variables with zero mean and standard deviation σ plus sinusoidal RFI with a specified amplitude and a uniformly distributed random phase. Although such an approach can be acceptable when calculating statistics for large samples containing many pulses, it does not realistically describe radars and other pulsed sources when resolved at higher time resolutions. Another signal model suggested in [7] is instead used in this study, and is reviewed here.

In this model, two different time scales are used. The first scale, N, denotes the number of samples on which the denominator and the square root of the numerator of the Shapiro-Wilk test are computed (the N in equation (1)). The longer scale consists of IN samples, and represents the radiometer integration period in samples. As described previously, I numerator and denominator values are obtained from the Shapiro-Wilk computations during an integration period, and then averaged and used to compute the W value for the entire sample.

For illustration, the sampling period of the digital radiometer system is assumed to be 16 nsec, and the integration period IN is taken as 32768 samples so that the total radiometer integration period is 524.288 μsec. The Shapiro-Wilk test length N is set to 4096 samples typically (i.e. 65.536 μsec); the effect of varying N is examined in Section IV-B.

For the case of pulsed sinusoidal RFI, sampled received fields can be written as [7]:

$$x_i[n] = A\cos(2\pi f_0\left[(i-i_0)N+n\right]+\phi)\mathcal{I}(n,i)+w_i[n] \quad n=0,1,\cdots,N-1, \quad i=0,1,\cdots,I-1 \tag{9}$$

where $w_i[n]$ refers to the independent identically distributed (i.i.d.) Gaussian measurements, with zero mean and standard deviation σ. The function

$$\mathcal{I}(n,i)=\begin{cases}1 & i_0N+N_s\le iN+n<i_0N+N_s+N_p\\ 0 & \text{otherwise}\end{cases} \tag{10}$$

is an "indicator" function that locates RFI containing samples. Here, i_0 is the pulse arrival "frame", A is the amplitude, f_0 is the frequency, and ϕ is the phase of a single sinusoidal pulse. It is assumed that if there are multiple pulses (i.e with arrival frames i_0, i_1, $\cdots$) within the IN sized sample, they have identical amplitudes A and durations N_p, but the frequency f_0, phase ϕ, and arrival sample N_s are chosen independently. These choices result in a duty cycle, d, of

$$d=\frac{N_{pulse}N_p}{IN} \tag{11}$$

where N_{pulse} is an integer.

As in [8], sine wave amplitudes in what follows are described in terms of the ratio R of the average "signal-to-noise" power ratio $(dA^2/\left(2\sigma^2\right))$ normalized by a factor proportional to the uncertainty in the radiometer power estimate $(\sigma^2/\sqrt{NI})$. This definition gives

$$R = \frac{dA^2}{2}\sqrt{NI} \tag{12}$$

$$A = \sqrt{\frac{2R}{d\sqrt{NI}}} \tag{13}$$

The parameter R thus describes the RFI power contribution to the integrated power in units proportional to the brightness standard deviation (i.e. NEDT). Typically RFI having $R>10$ would be readily detectable without additional detection procedures, so the primary interest is in detecting RFI having $R<10$.

B. Cases considered

Monte Carlo simulations were performed for fixed pulse amplitudes (R), duration (N_p), and number of pulses (N_{pulse}) in a frame of 32768 total samples. Pulse frequencies were uniformly distributed from $0<f_0<1/2$ and independent from pulse-to-pulse. Phases ϕ were also selected uniformly from 0 to 2π radians, and pulse arrival frames i_0 and arrival

sample N_s were also selected uniformly within the constraints required by the specified number of pulses and pulse durations (i.e. pulses were not allowed to overlap in time.)

The simulations performed were chosen to obtain a basic understanding of test performance in semi-realistic RFI situations. First, a case having ten pulses of length $N_p = 32$ (0.512 μsec) within the integration period of 524.288 μsec was considered to model sort pulse radar-like emissions at a very high pulse repetition frequency; the resulting duty cycle is approximately 1%, and simulations were performed for R values of 0 (false alarm case), 2.5, 5, and 10. Second, a case having a single pulse of length $N_p = 16384$ (i.e. 256.14 μsec) was used to obtain a 50% duty cycle which is of interest due to the blind spot encountered by kurtosis at this duty cycle. Such longer radar pulses are also produced by many radar systems, as evidenced by the data reported in [10]. R values used for 50% case were identical to those in the 1% duty cycle case. Finally, a case with a 100 percent duty cycle was used to model continuous RFI sources; in this case much larger R values of $0, 30, \cdots 120$ were required, as will be discussed in the next Section.

IV. Results

A. Histograms of W

The Monte Carlo simulation produces a set of W values for the cases described in Section III-B, which include both a false alarm simulation $R = 0$ and simulations when RFI is present. Histograms of the W values obtained for the $d \approx 1\%$ case are presented in Figure 2. The upper plot (no-quantization of y_i data) shows the concentration of W near 1 in the RFI free case, as expected, although the mean of the pdf when $R = 0$ is not exactly 1 [16] due to the finite sample size utilized in the test. Non-Gaussian behavior is indicated in the Shapiro-Wilk test when the test statistic value becomes significantly less than one; values of W less than a threshold t are therefore declared as containing RFI. This basic behavior of W is apparent in the Figure, where although the histograms of $R = 0$ and $R = 2.5$ are nearly identical, the histogram means become smaller with increasing R. A larger variance of the test statistic is also observed in this case as R is increased.

Histograms are also shown in the lower plot of Figure 2 when quantization effects of the y_i data are included. These data are generated by assuming that the RFI free noise has a standard deviation $\sigma = G$ and that the data are then rounded to integer values. Larger values of G therefore should lead to reduced quantization effects, although clipping would eventually become a problem for very large G values. A rule of thumb to avoid clipping is to select the number of bits for the RFI-free case such that signals with amplitudes at least 6 times G do not cause clipping. In practice, the value of G is determined by the ratio of the observed thermal noise voltage standard deviation to the bit width of the analog to digital converter used in the radiometer. The results show negligible differences between the histograms illustrated when quantization with $G = 4$ is considered. Quantization effects can become significant for $G < 4$; however such effects are not considered further as $G \geq 4$ is a reasonable expectation for many radiometer systems.

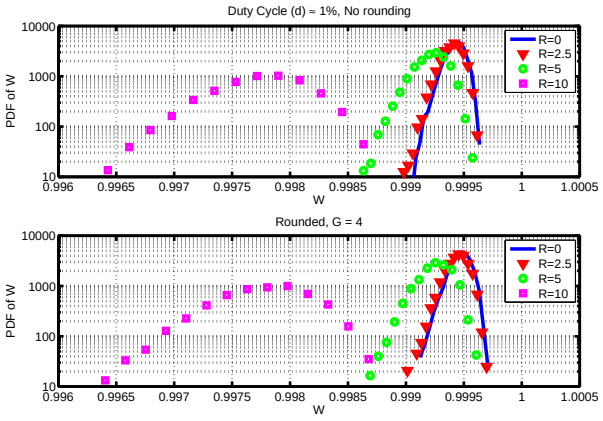

Fig. 2. Histograms (scaled to correspond to probability density functions) of W for non-quantized (upper Figure) and quantized data ($G = 4$, lower Figure), $d \approx 1\%$.

B. Receiver operating characteristic curves

Given the Monte Carlo set of W values, the probability of false alarm and probability of detection as a function of the threshold t in the test $W < t$ can be computed. Receiver operating characteristic (ROC) curves plotting the probability of detection versus the probability of false alarm as the threshold t is varied can then be produced.

Figure 3 illustrates the obtained ROC curve for the $d \approx 1\%$ case. The results show that the test has poor performance at detecting RFI with $R = 2.5$, but improved performance for $R = 5$. A further examination of quantization effects is also provided by including the corresponding ROC curves using G values of 2, 4, and 8. The results show a modest impact of quantization when $G = 2$ that becomes negligible for $G \geq 4$.

Equation (13) shows that, for a fixed R value, the RFI sine wave amplitude A is decreased as d is increased. This fact suggests that test performance may degrade for higher duty cycle interference. To examine this issue, Figures 4 and 5 plot the corresponding results for $d = 50\%$ and $d = 100\%$, respectively. For the $d = 100\%$ case in Figure 5, performance is relatively poor even with an R value of 60; other tests such as those described in [2] would likely be preferable for continuous sinusoidal interference. It is interesting to note however that the $d = 50\%$ case of Figure 4 shows performance comparable to that achieved for $d = 1\%$. This is due to the fact that detection is not only a function of d and R, but also of the relationship between the pulse duration (N_p) and the local test size N. Simulations using a large number of shorter pulses to achieve a 50% duty cycle showed that much higher R values were required to obtain good test performance. Both Figures 4 and 5 again show quantization of the y_i data to have minimal impacts when $G \geq 4$, although the impact is somewhat larger than in the $d \approx 1\%$ case.

To examine further the impact of N, ROC curves were computed for fixed R values as the sample size N was varied from 64 to 4096 (keeping the total integration period NI constant at 32768 samples). The results are shown in Figures 6 and 7 for the $d \approx 1\%$ ($R = 2.5$) and $d = 50\%$ ($R = 5$) cases,

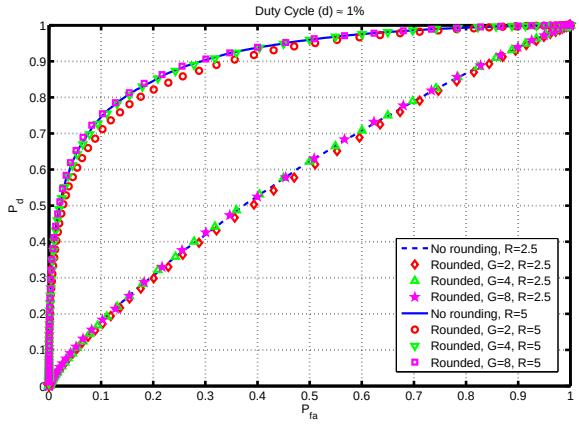

Fig. 3. ROC curves for $d \approx 1\%$

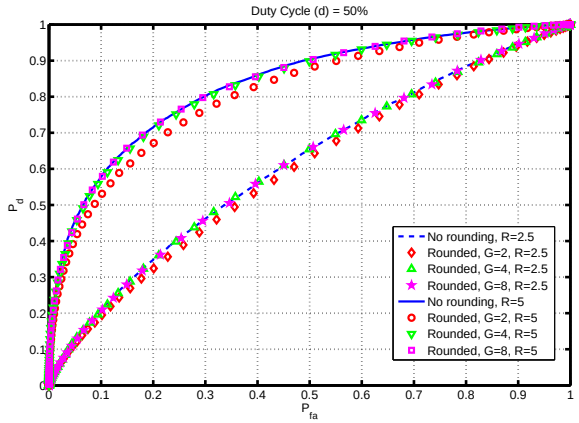

Fig. 4. ROC curves for $d = 50\%$

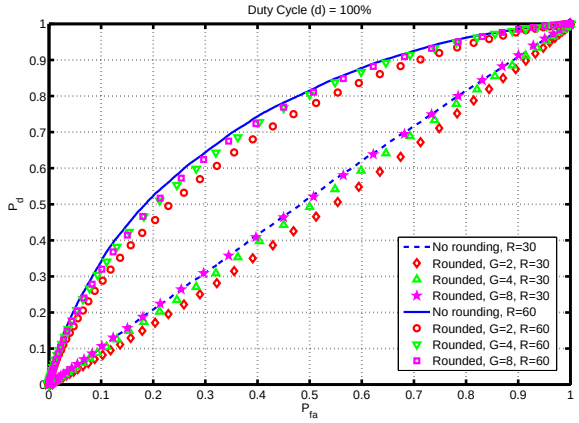

Fig. 5. ROC curves for $d = 100\%$

respectively. For $d \approx 1\%$, the best detection performance is obtained when $N = 64$, and performance degrades as N increases. This is not surprising since the pulses simulated in this case have length $N_p = 32$, so that the individual $N = 64$ sub-tests are more closely matched to the duration of the RFI pulses. The $d = 50\%$ cases instead shows improved performance as N becomes larger, again as might be expected since the RFI pulse in this case has a duration of 16384 samples. These results show that it is desirable to choose the sample size N to be matched to the duration of expected RFI pulses if this duration is known a-priori. In the absence of such information, the parameter N should be chosen as a trade-off between implementation complexity and test performance given any knowledge of a potential range of RFI pulse lengths. The results of the next section were computed using $N = 4096$ to represent the latter case.

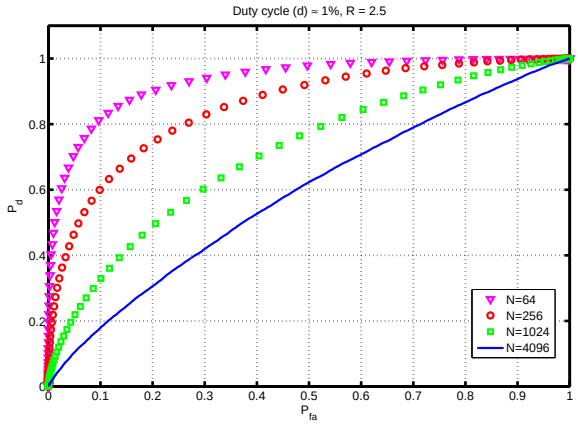

Fig. 6. ROC curves vs. test size N, R=2.5, $d \approx 1\%$

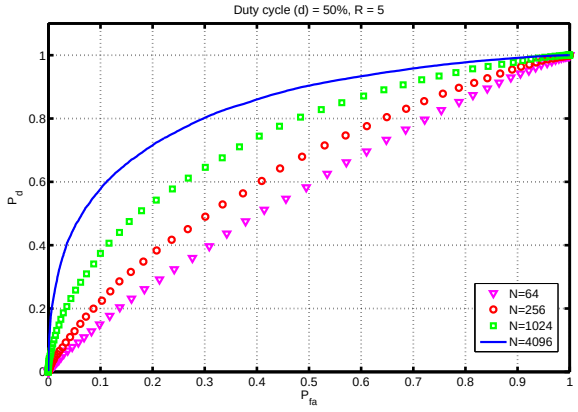

Fig. 7. ROC curves vs. test size N, R=5, $d = 50\%$

C. Comparison of ROC curves for the Shapiro-Wilk and kurtosis tests

Figures 8, 9, and 10 compare ROC curves achieved by the Shapiro-Wilk and kurtosis tests for the $d \approx 1$, 50, and 100 percent cases, respectively. ROC curves for the kurtosis test

were obtained from a Monte Carlo procedure under the same signal model as that used for the Shapiro-Wilk analysis. The kurtosis statistic was computed using the entire dataset of IN samples (i.e. no sub-sampling.) Subsampling of kurtosis may produce different results [10]-[11]; however, such an approach is not considered further because it would either require an increased system datarate (i.e. downlinking signals moments at a higher time rate) or would require floating-point operations onboard.

Results in Figure 8 show both tests to go from very poor performance to near perfect performance as R is varied from 2.5 to 10. In between these values, the kurtosis test achieves the better performance. The performance of the Shapiro-Wilk test can be improved to exceed that of the full sample kurtosis test if N is selected through an a-priori knowledge of the RFI pulse length, although kurtosis test performance could also be improved through the incorporation of temporal sub-sampling.

The situation is distinctly different in Figure 9 for duty cycle 50 percent, due to the "blind spot" of the kurtosis test in this case. The Shapiro-Wilk test retains sensitivity (although the results may be different for other choices of N and N_p as explained in Section IV-A), while the kurtosis test is insensitive to the presence of RFI.

Conclusions for the 100 percent duty cycle case in Figure 10 are similar to those in the one percent duty cycle case in that both tests go from poor to near perfect performance over a similar range of R values. Again the kurtosis test achieves better performance over this range. However, the required R value for good performance is quite high (up to 120) which suggests that the performance of both tests would likely be exceeded by other approaches.

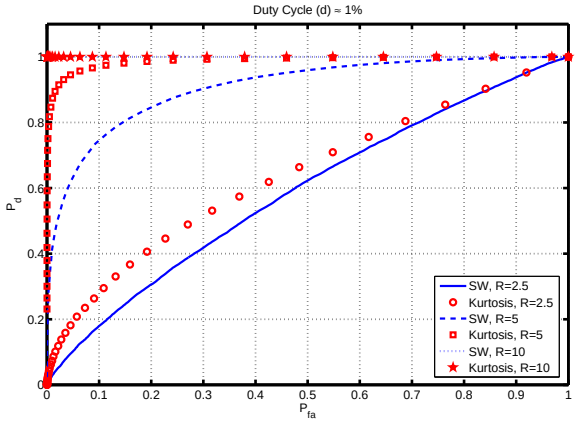

Fig. 8. Comparison of ROC curves for Shapiro-Wilk and Kurtosis tests, $d \approx 1\%$

V. Conclusions

The performance of the Shapiro-Wilk test for normality was analyzed in detecting pulsed sinusoidal RFI. Results showed that the test can be successful in detecting pulse sinusoidal RFI, particularly for duty cycles of 50% or less, and simulations not reported here over a larger range of duty cycles showed similar performance to those illustrated in

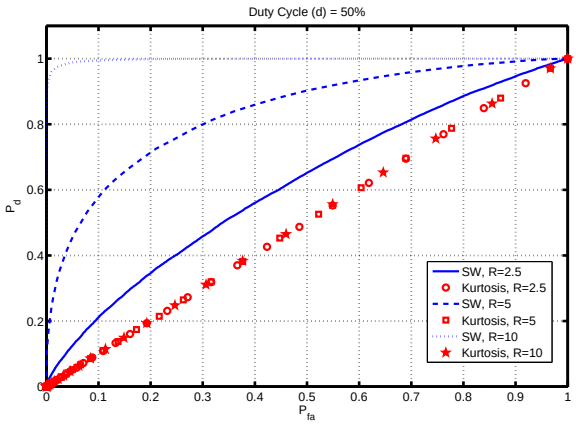

Fig. 9. Comparison of ROC curves for Shapiro-Wilk and Kurtosis tests, $d = 50\%$

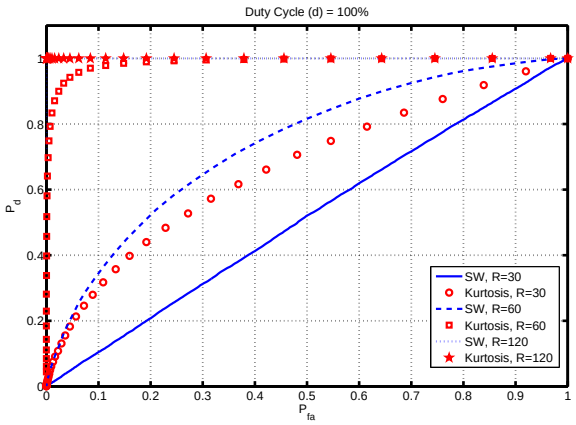

Fig. 10. Comparison of ROC curves for Shapiro-Wilk and Kurtosis tests, $d = 100\%$

Section IV. A comparison of results with those achieved by the kurtosis test showed that the two tests produce qualitatively similar results, with the kurtosis test generally achieving better performance in most cases. However, the Shapiro-Wilk test was shown not to suffer from the "blind spot" encountered in the kurtosis test at duty cycle 50 percent. It was also shown that Shapiro-Wilk test performance can be improved if a-priori expectations regarding RFI pulse lengths are available. Further investigations will be required to examine performance for other types of RFI, including sources producing "wideband" emissions that are more similar to Gaussian noise than the pulsed sine waves considered here.

Discussions of implementation of the Shapiro-Wilk test in hardware along with the effects of the quantization were also provided. Simulations showed that performance loss due to quantization is not significant if the radiometer thermal noise has a voltage standard deviation of approximately four times the analog to digital converter bit width. Implementation appears feasible, so that experimental tests should be possible in the future.

REFERENCES

[1] G. A. Hampson, S. W. Ellingson, and J. T. Johnson, "Design and demonstration of an interference suppressing microwave radiometer," *IEEE Aerospace Conference,* conference proceedings, vol.2, pp. 993-999, 2004

[2] B. Güner, J. T. Johnson, and N. Niamsuwan, "Time and frequency blanking for radio frequency interference mitigation in microwave radiometry," *IEEE Trans. Geosc. Rem. Sens.,* vol. 45, pp. 3672–3679, 2007.

[3] J. T. Johnson, A. J. Gasiewski, B. Güner, G. A. Hampson, S. W. Ellingson, R. Krishnamachari, N. Niamsuwan, E. McIntyre, M. Klein, and V. Y. Leuski, "Airborne radio-frequency interference studies at C-band using a digital receiver," *IEEE Trans. Geosc. Rem. Sens.,* vol. 44, pp. 1974-1985, 2006.

[4] C. S. Ruf, S. M. Gross, and S. Misra, "RFI detection and mitigation for microwave radiometry with an agile digital detector," *IEEE Trans. Geosc. Rem. Sens.,* vol. 44, pp. 694-706, 2006.

[5] S. Misra, S. S. Kristensen, S. S. Sobjaerg, and N. Skou, "CoSMOS: Performance of kurtosis algorithm for radio frequency interference detection and mitigation," *IGARSS 2007,* conference proceedings, 2007.

[6] N. Niamsuwan, J. T. Johnson, and S. W. Ellingson, "Examination of a simple pulse blanking technique for RFI mitigation" *Radio Science,* vol. 40, June 2005.

[7] J. T. Johnson and L. C. Potter, "A study of algorithms for detecting pulsed sinusoidal interference in microwave radiometry," submitted to *IEEE Trans. Geosc. Rem. Sens.,* 2007.

[8] R. D. De Roo, S. Misra, and C. S. Ruf, "Sensitivity of the kurtosis statistics as a detector of pulsed sinusoidal RFI," *IEEE Trans. Geosc. Rem. Sens.,* vol. 45, pp. 1938–1946, 2007.

[9] J. R. Piepmeier, P. Mohammed, and J. Knuble, "A Double Detector for RFI Mitigation in Microwave Radiometers," *IEEE Trans. Geosc. Rem. Sens.,* vol. 46, pp. 458–465, 2008.

[10] P. N. Mohammed, J. Knuble and J. Piepmeier, "Pulse and kurtosis detection of radio-frequency interference (RFI): an experimental comparison," *IGARSS 2008,* conference proceedings, 2008.

[11] S. Misra and C. Ruf, "Comparison of pulsed sinusoidal RFI detection algorithms using time and frequency sub-sampling" *IGARSS 2008,* conference proceedings, 2008.

[12] R. DeRoo and S. Misra, "Effectiveness of the sixth moment to eliminate a kurtosis blind spot in the detection of interference in a radiometer," *IGARSS 2008,* conference proceedings, 2008.

[13] S. M. Kay, *Fundamentals of Statistical Signal Processing: Volume II, Detection Theory,* Upper Saddle Creek, NJ: Prentice Hall, 1998.

[14] R. Fisher, "The moments of the distribution for normal samples of measures of departures from normality," *Proc. Royal Soc. A*, vol. 130, pp. 16–28, 1930.

[15] E. Pearson, "A further development of tests for normality," *Biometrika,* vol. 22, pp. 239–249, 1930.

[16] S. S. Shapiro and M. B. Wilk, "An analysis of variance test for normality (complete samples)," *Biometrika,* vol. 52, pp. 591–611, 1965.

[17] S. S. Shapiro, M. B. Wilk, and H. J. Chen, "A comparative study of various tests for normality," *Journal of the American Statistical Association,* vol. 63, pp. 1343–1372, 1968.

[18] E. Seier, "Comparison of tests for univariate normality," *Interstat Stat. Journal,* available at `http://interstat.statjournals.net/YEAR/2002/articles/0201001.pdf`, 2002.

[19] F. F. Gan and K. J. Koehler, "Goodness of Fit Tests Based on P-P Probability Plots," *Technometrics,* vol. 32, pp 289–303, 1990.

[20] S. S. Shapiro and R. S. Francia, "Approximate analysis of variance test for normality," *J. Am. Statist. Assoc.* vol. 67, pp. 215-25, 1972.

[21] L. Chen and S. S. Shapiro, "An Alternative test for normality based on normalized spacings," *J. of Stat. Comput. and Sim.,* vol. 53, pp. 269-287, 1995.

[22] B. Güner, M. Frankford and J. T. Johnson, "Comparison of three omnibus normality tests for the detection of pulsed sinusoidal RFI sources," *submitted to URSI General Assembly 2008*.

[23] C. Jarque and A. Bera, "Efficient tests for nonlinearity, heteroskedasticity, and serial independence of regression residuals," *Economics Letters,* vol. 6, pp. 255-259, 1980.

[24] A. Bera and C. Jarque, "A test for normality of observations and regression residuals," *Int'l. Stat. Rev.,* vol. 55, pp. 163-172, 1987.

[25] J. P. Royston, "Approximating the Shapiro-Wilk W-test for non-normality," *Statistics and Computing,* vol. 2, pp. 117–119, 1992.

[26] G. Blom, *Statistical estimates and transformed Beta-variables,* New York: John Wiley and Sons, Inc, 1958.

[27] H. L. Harter, "Expected values of normal order statistics," *Biometrika,* vol. 48, pp. 151–165, 1961.

[28] J. Harkins, T. El-Ghazawi, E. El-Araby, and M. Huang, "Performance and analysis of sorting algorithms on the SRC 6 reconfigurable computer," *IEEE Field Programmable Technology Con. Proc.,*, pp. 295–296, 2005.

[29] J. P. Royston, "Correcting the Shapiro-Wilk W for ties," *Journal of Computation and Simulation,* vol. 31, pp. 237–249, 1989.

[30] J. P. Royston, "An extension of Shapiro and Wilk's W test for normality to large samples," *Applied Statistics,* vol. 31, pp. 115–124, 1982.

[31] J. P. Royston, "A toolkit for testing for non-normality in complete and censored samples," *The Statistician,* vol. 42, pp. 37–43, 1993.